Theoretical prediction of different decomposition paths for $Ca(BH_4)_2$ and $Mg(BH_4)_2$

Yongsheng Zhang,[1] Eric Majzoub,[2] Vidvuds Ozoliņš,[3] and Chris Wolverton[1]
[1]*Department of Materials Science & Engineering, Northwestern University, Evanston, Illinois 60208, USA*
[2]*Center for Nanoscience, Department of Physics and Astronomy, University of Missouri, St. Louis, Missouri 63121-4400, USA*
[3]*Department of Materials Science & Engineering, University of California, Los Angeles, California 90095-1595, USA*
(Received 31 August 2010; published 9 November 2010)

We have studied the decomposition pathways of both Ca- and Mg-borohydride using density-functional theory (DFT) calculations of the free energy (including vibrational contributions) in conjunction with a Monte Carlo-based crystal-structure prediction method, the prototype electrostatic ground-state (PEGS) search method. We find that a recently proposed CaB_2H_2 intermediate [M. D. Riktor, M. H. Sørby, K. Chłopek, M. Fichtner, and B. C. Hauback, J. Mater. Chem. **19**, 2754 (2009)] is energetically highly unfavorable and hence very unlikely to form. We systematically search for low-energy structures of CaB_2H_n compounds with $n=2$, 4, and 6 using PEGS simulations, refining the resulting structures with accurate DFT calculations. We find that the lowest-energy CaB_2H_2 and CaB_2H_4 crystal structures do not lie on the thermodynamically stable decomposition path but rather are unstable with respect to a decomposition pathway involving the previously proposed $CaB_{12}H_{12}$ phase. We also predict a CaB_2H_6 compound which forms a low-energy intermediate in the calcium borohydride decomposition pathway. This new reaction pathway is practically degenerate with decomposition into the $CaB_{12}H_{12}$ phase. Similar calculations for magnesium borohydride show that a recently predicted MgB_2H_6 phase does not form a stable intermediate in the decomposition pathway of $Mg(BH_4)_2$.

DOI: 10.1103/PhysRevB.82.174107 PACS number(s): 61.50.Ah, 61.66.Fn, 63.20.−e, 65.40.−b

I. INTRODUCTION

Metal borohydrides[1,2] [$M(BH_4)_n$, where M is an alkali or alkaline-earth metal] are receiving considerable attention as hydrogen storage materials due to their high gravimetric capacities of hydrogen. In particular, the most widely studied compounds in this class, $LiBH_4$ (Refs. 3–6) (18.3 wt %), $Mg(BH_4)_2$ (Refs. 7–9) (11.9 wt %), and $Ca(BH_4)_2$ (Refs. 10 and 11) (11.6 wt %), all exhibit theoretical hydrogen content above the system target for passenger vehicles.[2,12] Unfortunately, for vehicle applications, the temperatures of hydrogen release for the compounds are often high enough that hydrogen cannot be extracted using waste heat from proton-exchange membrane fuel cells operating at approximately 80 °C. Therefore, recent research has concentrated on clarifying the physical and chemical factors that determine the decomposition temperatures of borohydrides.

The temperatures and pressures of hydrogen desorption and absorption are dependent on the thermodynamics and kinetics of the favored reaction pathways. For the alkaline-earth borohydrides, $Ca(BH_4)_2$ and $Mg(BH_4)_2$, simple one-step decomposition reactions might proceed according to

$$Mg(BH_4)_2 \rightarrow MgB_2 + 4H_2,$$

$$Ca(BH_4)_2 \rightarrow \frac{2}{3}CaH_2 + \frac{1}{3}CaB_6 + \frac{10}{3}H_2. \quad (1)$$

Until a few years ago, it was generally assumed that borohydride decomposition proceeds according to the simple pathways above. However, several intermediate compounds have recently been suggested to appear in the decomposition reactions of borohydrides.[3,13–17] The existence of these intermediates changes the preferred reaction sequence and hence the thermodynamics of hydrogen release. Hence, it is crucial to have a good understanding of the stability and thermodynamics of these (and other) reaction intermediates.

The existence of intermediates will involve many different possible borane chemistries.[18–20] Recent experimental[14,16] and theoretical[3,13] studies indicate that the decomposition pathways are not simple one-step reactions [Eq. (1)] but instead may be a multistep decomposition path. The formation of icosahedral $[B_{12}H_{12}]^{2-}$ anion complexes has been identified in the $LiBH_4$ and $Mg(BH_4)_2$ decomposition reactions by nuclear magnetic resonance,[17,21] but to date, not in the $Ca(BH_4)_2$ decomposition. Subsequently, using density-functional theory (DFT) calculations, Ozoliņš *et al.*[13] confirmed that the $[B_{12}H_{12}]^{2-}$ compounds are stable intermediates in the Li and Mg systems and also predicted the existence of a yet unobserved $CaB_{12}H_{12}$ compound. The DFT calculations showed the thermodynamics of decomposition into $CaB_{12}H_{12}$ are nearly degenerate with decomposition directly into CaH_2 according to Eq. (1), providing an explanation for the difficulty of observing this phase. More recently, two experimental papers[14,22] have observed new intermediate phases CaB_mH_n by x-ray diffraction (XRD) in the decomposition of $Ca(BH_4)_2$. Riktor *et al.*[14] observe an intermediate phase during decomposition and suggest that the stoichiometry of this phase is CaB_2H_n (where the authors could not definitively determine the value of $n<8$). From the experimental XRD pattern, the authors do suggest a possible structure for the intermediate with a value of $n=2$, i.e., CaB_2H_2. In another paper, Lee *et al.*[22] report the existence of an intermediate phase, CaB_mH_n, of unknown stoichiometry. For $Mg(BH_4)_2$, Setten *et al.*[15] used DFT molecular dynamics on $Mg(BH_4)_2$ with several hydrogen vacancies and identified MgB_2H_6 as a possible intermediate compound. There are still many unanswered questions regarding the stability of intermediates in these systems and one would like to gain a more complete understanding of the stoichiometries, crystal structures, and reaction thermodynamics of these intermediates.

In this paper, we study both previously proposed reaction intermediates and also predict several intermediate structures and stoichiometries. We use DFT calculations to obtain total crystal binding energies and vibrational free energies, as well as the prototype electrostatic ground-state (PEGS) search method[23] to predict the unknown crystal structures of possible intermediates. Our calculations yield distinct insight into the thermodynamics, crystal structures, and stoichiometries of the thermodynamically preferred decomposition pathways of $Ca(BH_4)_2$ and $Mg(BH_4)_2$. We find that the experimentally proposed CaB_2H_2 crystal structure is very high in energy and we predict a CaB_2H_6 compound as a possible stable intermediate product in the decomposition sequence of $Ca(BH_4)_2$. On the other hand, we find no evidence for a stable MgB_2H_6 intermediate in the decomposition of $Mg(BH_4)_2$.

II. METHODOLOGY

We perform DFT calculations using the Vienna *ab initio* simulation package (VASP) code with the projector-augmented wave scheme[24] and the generalized-gradient approximation of Perdew, Burke, and Ernzerhof[25] (GGA-PBE) for the electronic exchange-correlation functional. The energy cutoff for the plane-wave expansion is 800 eV. We treat $3s^2$, $3s^23p^64s^2$, and $2s^22p^1$ as valence electrons in Mg, Ca, and B atoms, respectively. The Brillouin zones are sampled by Monkhorst-Pack[26] k-point meshes for all compounds with meshes chosen to give a roughly constant density of k points (20 Å^3) for all compounds. Tests showed that our choice of k points yield energies that are converged to within 0.01 eV/(f.u.). Atomic positions and the unit cell are both relaxed until all the forces and components of the stress tensor are below 0.01 eV/Å and 0.2 kbar, respectively. Phonons are calculated using the supercell force-constant method (as implemented in the program described in Refs. 27 and 28) and the vibrational entropies and enthalpies are obtained by directly summing over the calculated phonon frequencies.

For this paper, we wish to predict crystal structures for a wide range of candidate intermediate compounds and stoichiometries. While DFT calculations are typically quite accurate for these hydride systems, a direct prediction of unknown crystal structures from DFT is computationally prohibitive due to the large configuration space which must be explored. For this crystal-structure prediction task, we turn to the PEGS search method.[23] In the PEGS method, the borohydride system is described by a combination of an electrostatic potential and soft-sphere repulsion

$$E_{\mathrm{tot}}^{\mathrm{PEGS}} = \sum_{i>j} \frac{Q_i Q_j}{d_{ij}} + \sum_{i>j} \frac{1}{d_{ij}^{12}}, \tag{2}$$

where, each atom i is represented by a radius (R_i) and a charge (Q_i), d_{ij} is the separation distance between atoms i and j, and the first and second terms are the Coulomb energy and the repulsive soft-sphere potential to prevent the systems from collapsing. The Coulomb interactions are calculated for all pairs of atoms, regardless of distance, while the soft-sphere interactions are only nonzero when atomic spheres (R) overlap. The cation ionic radii of Ca and Mg (R_{Ca} =0.99 Å, R_{Mg}=0.65 Å) are taken from standard sources[29] and their ionic charges are $+2e$. For the anion groups, the B ionic radius is determined by the difference of d (cation-B) and R_{cation}, where the value of d is obtained from experimental structures or the best structure from PEGS+DFT determinations at 1 formula unit (f.u.) and the H radius is further tuned to get the lowest final DFT relaxed energies based on PEGS outputs. The charges distributed on atoms in the anion group are computed by the GAMESS cluster code.[30] All anion group parameters are given in Table I.

TABLE I. The parameters of cations and anion groups, radii (R), and charges (Q), using in PEGS simulations.

Cation	R_{Mg} (Å)	Q_{Mg} (e)	R_{Ca} (Å)	Q_{Ca} (e)
	0.65	+2.0	0.99	+2.0
Anion	R_{B} (Å)	Q_{B} (e)	R_{H} (Å)	Q_{H} (e)
$[B_2H_2]^{2-}$	2.0	−0.845	1.45	−0.155
$[B_2H_4]^{2-}$	2.0	−0.625	1.45	−0.188
$[B_2H_6]^{2-}$	1.9	−0.016	1.50	−0.328

After setting up the PEGS input parameters, this computationally inexpensive electrostatic+repulsive potential [Eq. (2)] is then used in Monte Carlo (MC) simulations. We applied 30 PEGS annealing simulations with different initial random seeds for each stoichiometry of varying 1–4 f.u. During PEGS simulations, we keep the anion group as a rigid unit. In the MC simulation, the MC trial moves include cation atom displacements, anion group displacements, anion group rotations, cation/anion swaps, and unit-cell vector distortions and volume changes.[23] We emphasize that our PEGS+MC method explores many possible cell shapes, volumes, and bonding topologies for a given number of formula units in the unit cell and that no knowledge of the bonding geometries is used beyond the geometry of the complex anions and the ionic radii.

For the $[B_2H_2]^{2-}$ and $[B_2H_4]^{2-}$ anions, we must first determine the geometry of the anion group. Our DFT computed structures (see below) show B-B chains in the solid phase. Hence, we make a very general choice for the anion geometry by using two $[BH]^-$ and $[BH_2]^-$ anion groups in a cell to mimic the $[B_2H_2]^{2-}$ and $[B_2H_4]^{2-}$ anions, respectively. For the $[B_2H_6]^{2-}$ anion, there is a well-known B_2H_6 molecular geometry structure of the gas phase (point group: D_{2h}) (Refs. 20 and 31–34) (Fig. 1). It is an electron-deficient molecule with H bridging.[18,20] However, under a charged background ($-2e$), $[B_2H_6]^{2-}$ is isoelectronic with C_2H_6 (point group: D_{3d}) (Ref. 35) and adopts the ethanelike structure in Fig. 1. Before running PEGS simulations, we tested the stability of this gas phase B_2H_6 molecular structure and confirmed its bridged geometry is only stable in the neutral case (gas phase), but when given a $-2e$ charge background (in GAMESS), its geometry indeed distorts to the ethanelike structure (Fig. 1). We confirm the suitability of this ethanelike structure in a further test, in which we put one Ca and two

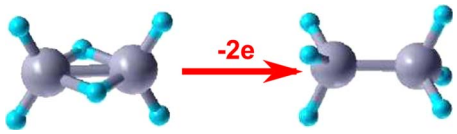

FIG. 1. (Color online) Schematic of B_2H_6 molecular geometry in the gas phase (left) and an ethanelike structure under a charged ($-2e$) background (right). Gray spheres and small spheres represent B atoms and H atoms, respectively.

$[BH_3]^-$ in a cell. After DFT relaxation within VASP, these two $[BH_3]^-$ bond to each other to form the ethanelike structure. Therefore, we take this ethanelike structure to mimic the $[B_2H_6]^{2-}$ anion group geometry in our subsequent PEGS calculations.

Although PEGS Monte Carlo simulations provide many candidate structures, its electrostatic potential is too crude to be used alone to predict quantitatively accurate crystal structures. Hence, accurate methods such as DFT calculations are needed to carry out a full relaxation of the PEGS output structures. We perform DFT calculations on all structures that result from PEGS and select the compounds with the lowest DFT energies as the most promising stable structures.

III. AN INTERMEDIATE PUZZLE: CaB_2H_2

In a recent study by Riktor *et al.*,[14] CaB_2H_n ($n<8$) is identified as an intermediate compound in the decomposition of $Ca(BH_4)_2$ by XRD; the same authors suggest that the most probable composition is $n=2$, i.e., CaB_2H_2. The CaB_2H_2 structure proposed by Riktor *et al.*[14] belongs to the *Pnma* space group (the left panel in Fig. 2) and fits the measured XRD pattern very well. The structure forms $-BH_2-BH_2-$ chains and, somewhat surprisingly, has interstitial B atoms

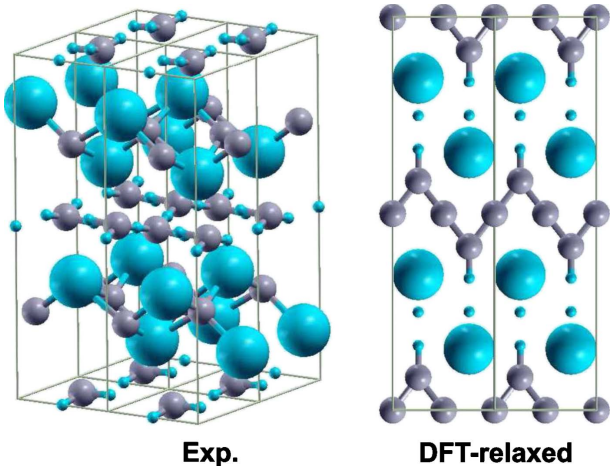

FIG. 2. (Color online) Schematic view of the CaB_2H_2 experimental crystal structure (the left panel) and corresponding DFT fully relaxed structure (the right panel). The former one has the *Pnma* space group with lattice constants $a=12.81$ Å, $b=4.08$ Å, $c=3.90$ Å. While the latter one after the relaxation shows $a=14.92$ Å, $b=3.88$ Å, $c=3.71$ Å. Big spheres, gray spheres and small spheres represent Ca atoms, B atoms, and H atoms, respectively.

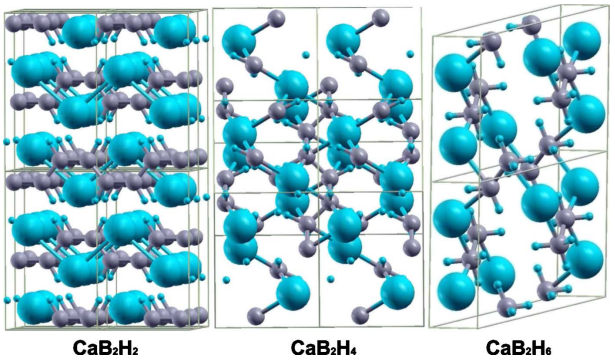

FIG. 3. (Color online) Schematic view of the lowest-energy structures of CaB_2H_n ($n=2,4,6$) by PEGS+DFT predictions. Detailed structural information, lattice parameters, and atomic positions are given in Table II.

that do not bond to any H atoms. The two symmetry-inequivalent bond lengths of Ca-B are 2.21/2.29 and the two bonds of B-H are 1.07/1.22 Å. We performed DFT calculations for this CaB_2H_2 compound both in the experimental geometry and with fully relaxed atomic positions and unit-cell vectors. Our DFT calculations suggest that the crystal structure of CaB_2H_2 proposed in Ref. 14 is incorrect. Indeed, DFT relaxation of this structure results in a bonding geometry (the right panel in Fig. 2) that is *qualitatively* different from the experimental geometry. For example, after DFT relaxation the interstitial B atoms exchange with H in the middle of $-BH_2-BH_2-$ chains to form B chains with a B-B bond length of 1.58 Å. The Ca-B bond length increases dramatically to 2.89 Å and B-H bond length is 1.20 Å. The DFT energy of the relaxed structure is ~579 kJ/(mol f.u.) lower than that of the original experimental geometry. The large change in energy upon relaxation suggests the starting structure is not optimal. For instance, taking the experimental MgH_2 (Ref. 36) and CaH_2 (Ref. 37) crystal structures, DFT relaxation lowers their energy by only 0.05 kJ/(mol f.u.) and 0.1 kJ/(mol f.u.), respectively. Given such enormous inconsistencies between the experimental structure and the DFT calculations of CaB_2H_2, we suggest that the structure and stoichiometry of this intermediate phase should be the subject of additional future experimental studies.

IV. THEORETICAL PREDICTION OF CaB_2H_n CRYSTAL STRUCTURES, $n=2,4,6$

To help search for new, low-energy crystal structures at the CaB_2H_2 stoichiometry, we use the combination of PEGS+DFT to guide our search. The PEGS+DFT lowest energy structure of CaB_2H_2 (the left panel in Fig. 3) has a *Cmcm* space group (Table II), Ca-B bond length of 2.85 Å, B-B bond length of 1.66 Å, and B-H bond length of 1.26 Å. In the PEGS+DFT CaB_2H_2 structure, the [BH] units combine with each other to form -B-B- chains (the left panel in Fig. 3) and H atoms remain bonded to the corresponding B atoms. This PEGS+DFT structure is more than 96 kJ/(mol f.u.) lower than the experimentally proposed

TABLE II. PEGS+DFT predicted crystal structures of *Cmcm* CaB_2H_2 (space group 63, the left panel in Fig. 3), $C2/c$ CaB_2H_4 (space group 15, the middle panel in Fig. 3), and $C2/c$ CaB_2H_6 (space group 15, the right panel in Fig. 3). The lattice parameters of the *Cmcm* CaB_2H_2, $C2/c$ CaB_2H_4 and $C2/c$ CaB_2H_6 are: a =4.11 Å, b=9.32 Å, c=5.45 Å; a=9.07 Å, b=5.89 Å, c =5.63 Å, β=54.85°; a=7.09 Å, b=7.16 Å, c=7.33 Å, β =76.29°, respectively.

Atom	Wyckoff position	x	y	z
		Cmcm CaB_2H_2		
Ca	4*c*	0.0000	0.3700	0.2500
B	8*f*	0.0000	0.0689	0.4033
H	8*f*	0.0000	0.1856	0.9816
		$C2/c$ CaB_2H_4		
Ca	4*c*	0.2500	0.2500	0.9338
B	8*f*	0.9630	0.3906	0.6519
H	8*f*	0.9880	0.1957	0.0019
H	8*f*	0.7931	0.3903	0.0879
		$C2/c$ CaB_2H_6		
Ca	4*e*	0.0000	0.4451	0.2500
B	8*f*	0.2024	0.3189	0.9231
H	8*f*	0.2268	0.4880	0.9484
H	8*f*	0.2686	0.2964	0.7528
H	8*f*	0.0250	0.2913	0.9469

CaB_2H_2 structure[14] (even after the large atomic relaxation of this structure). However, we note that our lower energy PEGS+DFT CaB_2H_2 structure does not reproduce the experimental XRD pattern. Also, the DFT electronic densities of states (eDOS) show that both the experimental and PEGS+DFT CaB_2H_2 crystal structures are metallic, which is somewhat unexpected given the highly ionic character of known stable borohydrides.

To supplement the crystal structures of CaB_2H_2 found from the PEGS+DFT method, we also searched for prototype structures for CaB_2H_2 from the International Crystal Structure Database. The structure prototypes and symmetries found were: $EuIr_2B_2$ (*Fddd*); $CeIr_2B_2$ (*Fddd*); $CaIr_2B_2$ (*Fddd*); CoW_2B_2 (*Immm*); YCo_2B_2 (*I*4/*mmm*); $LaCo_2B_2$ (*I*4/*mmm*); Ni_2TbB_2 ($C2/c$); Mo_2NiB_2 (*Immm*); YIr_2B_2 (*Fddd*); $CaMg_2N_2$ (*P*3*m*1); $CaNi_2As_2$ (*I*4/*mmm*); $CaAl_2Si_2$ (*P*3-*m*1); $CaCo_2P_2$ (*I*4/*mmm*); Ca_2 (Be_4N_4); (*I*4/*mcm*); Ca_2GeN_2 (*P*4$_2$/*mbc*); $CaRh_2B_2$ (*Fddd*). Structural optimizations and total-energy DFT calculations for all of the structure prototypes were carried out twice with H and B atom positions switched due to the inherent ambiguity in the prototype structure for those positions. After structural optimization, the database structure type with the lowest total energy was Ni_2TbB_2 with space group $C2/c$. However, this structure was still about 48 kJ/(mol f.u.) higher in energy than the PEGS structure with space group *Cmcm*.

As we mentioned above, the value of n=2 in the experimental CaB_2H_n intermediate stoichiometry is only one possibility in the decomposition of $Ca(BH_4)_2$.[14] Hence, we further investigate the cases of n=4 and 6, i.e., CaB_2H_4 and CaB_2H_6. Our PEGS+DFT lowest energy structures for CaB_2H_4 (the middle panel in Fig. 3) and CaB_2H_6 (the right panel in Fig. 3) both have the $C2/c$ space group (Table II). As in the PEGS-predicted CaB_2H_2 structure, CaB_2H_4 also contains -B-B- chains with bond lengths of 1.77/1.80 Å, which is similar to the B-B bond lengths in the $[B_{12}H_{12}]^{2-}$ anion group. The B-H bond length in our CaB_2H_4 structure is 1.26/1.27 Å. In this structure, the BH bonds in the $[B_2H_4]^{2-}$ geometry are staggered in order to avoid strong HH repulsion. For most stoichiometries and low-energy crystal structures we have explored in borohydrides, we find that (whenever possible), B atoms prefer to bond each other to form chains (like in $[B_2H_2]^{2-}$ and $[B_2H_4]^{2-}$) or clusters (like in B bulk and $[B_{12}H_{12}]^{2-}$).

In contrast, -B-B- chains do not appear in our predicted CaB_2H_6 structure due to two reasons. One is electrostatics: the interactions between H are repulsive because of negative charges on H atoms (Table I). The other reason is the geometry: from the $[B_2H_6]^{2-}$ structure (Fig. 1), it is clear that each B is surrounded by three H atoms and one B atom. This type of binding environment, similar to $[BH_4]^-$, consists of a relatively compact cluster which cannot be easily penetrated by other ions. Therefore, the three H atoms at the end of each $[B_2H_6]^{2-}$ unit prevent them from approaching each other. The B-B and B-H bond lengths in this crystal structure are 1.75 and 1.24 Å, which are similar to other candidate borohydride intermediates, such as $[B_{12}H_{12}]^{2-}$ and our theoretically predicated $[B_2H_4]^{2-}$. Unlike the metallic properties in CaB_2H_2, the DFT eDOS of these CaB_2H_4 and CaB_2H_6 lowest energy structures show insulating properties with 2.18 eV and 4.57 eV band gaps, respectively. Still, we should note that none of our predicted CaB_2H_n (n=2,4,6) structures reproduces the experimental XRD patterns.[14,22]

V. DFT THERMODYNAMICS OF PROPOSED $Ca(BH_4)_2$ DECOMPOSITION PATHWAYS

As discussed above, multiple decomposition steps have been suggested in the decomposition of $Ca(BH_4)_2$ by experimental and theoretical studies, but the stable intermediate products and reactions are still unclear. In the previous section, we have predicted low-energy structures of possible intermediate compounds of CaB_2H_n (n=2,4,6). In order to help understand the thermodynamics of $Ca(BH_4)_2$ decomposition, we calculate the reaction enthalpies (Table III) of these new reaction pathways together with the well studied reactions to $CaB_{12}H_{12}$, CaB_6, or CaH_2 in Ref. 13. We note that there are small differences [~8 kJ/(mol H_2)] between our calculations for reaction enthalpies for decomposition into CaH_2—[reaction (2)] and $CaB_{12}H_{12}$—[reaction (3)] and from those calculated in Ref. 13. The differences are due to the use of different potentials and exchange-correlation functionals in the DFT computations. We performed tests using the same DFT setup as in Ref. 13 and find our reaction enthalpies are in excellent agreement with these previous calculations to within 1 kJ/(mol H_2).

In order to determine the lowest-energy reaction pathways, we plot the H_2 release enthalpies of each reaction pathway versus the number of moles of desorbed H_2. Connecting the lowest energies on this plot, one can form a

TABLE III. The reaction enthalpies of $Ca(BH_4)_2$ and $Mg(BH_4)_2$ decomposition through different pathways. $\Delta H_{\text{static}}^{T=0\ \text{K}}$ is the static enthalpy ignoring the zero-point energy. $\Delta H_{\text{ZPE}}^{T=0\ \text{K}}$ and $\Delta H^{T=300\ \text{K}}$ are the calculated enthalpies at $T=0$ K and 300 K, including the vibrational energies. The units of enthalpies and entropies are in kJ/(mol H_2) and J/(K mol H_2). T_c is the predicted critical temperatures at $p=1$ bar H_2 pressure using the van's Hoff equation ($\ln p=-\Delta H/RT+\Delta S/R$), and its unit is in degree Celsius (°C).

Reaction path	$\Delta H_{\text{static}}^{T=0\ \text{K}}$	$\Delta H_{\text{ZPE}}^{T=0\ \text{K}}$	$\Delta H^{T=300\ \text{K}}$	$\Delta S^{T=300\ \text{K}}$	T_c
(1) $CaH_2+2B+3H_2$	71.56				
(2) $\frac{1}{3}CaB_6+\frac{2}{3}CaH_2+\frac{10}{3}H_2$	53.75	31.66	37.04	108.51	68
(3) $\frac{1}{6}CaB_{12}H_{12}+\frac{5}{6}CaH_2+\frac{13}{6}H_2$	49.69	27.33	31.34	92.50	66
(4) $CaB_2H_2+3H_2$	68.51				
(5) $CaB_2H_4+2H_2$	77.35				
(6) $CaB_2H_6+H_2$	44.04	28.43	31.09	83.19	100
(7) MgB_2+4H_2	49.86	28.34	41.79	110.88	104
(8) $\frac{1}{6}MgB_{12}H_{12}+\frac{5}{6}MgH_2+\frac{13}{6}H_2$	43.37	19.47	24.14	103.76	−40
(9) $MgB_2H_6+H_2$	64.99	45.96	49.94	95.18	251

"hull" which is convex downward. The stable equilibrium phases must fall on this convex hull. Any energy above the linear combination of adjacent phases would indicate an instability toward phase separation into these two neighboring phases. For the case of static $T=0$ K energies (without zero-point energies), without considering our predicted CaB_2H_n phases at first, we see that the lowest-energy reactions pathways for the decomposition of $Ca(BH_4)_2$ involve the following stable intermediates and reactions: $CaB_{12}H_{12}$—[reaction (3)] and CaB_6—[reaction (2)]. These phases fall on a low-energy decomposition sequence for $Ca(BH_4)_2$ in Fig. 4 (black dashed line). The low energy of these decomposition

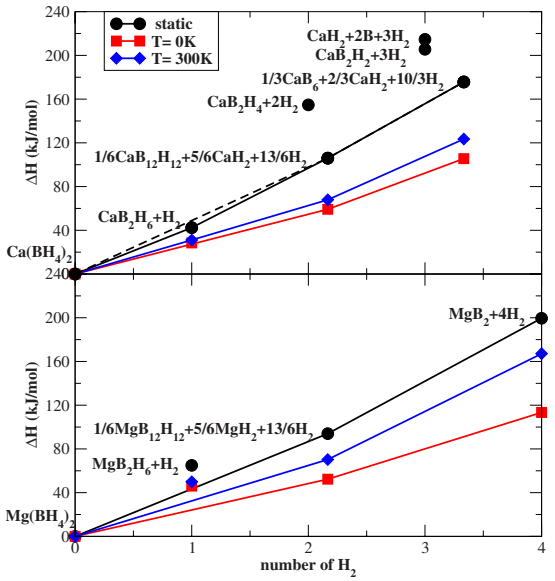

FIG. 4. (Color online) Theoretical prediction of decomposition pathways in $Ca(BH_4)_2$ (upper panel) and $Mg(BH_4)_2$ (lower panel) based on the calculated reaction enthalpies in Table III. The black circle/line, the red square/line, and the blue diamond/line represent the convex hulls of static enthalpies at $T=0$ K, enthalpies including the vibrational energies at $T=0$ K and $T=300$ K, respectively. The black dashed line is the convex hull without involving CaB_2H_n reactions in at the static energy case.

reactions is good agreement with the results in Ref. 13. However, including our predicted CaB_2H_n phases in the same plot (black solid line in Fig. 4), the reaction pathway to CaB_2H_6—[reaction (6)] clearly breaks the previous convex hull linking $Ca(BH_4)_2$ with $CaB_{12}H_{12}$—[reaction (3)], which indicates that our predicted CaB_2H_6 phase is a possible intermediate that would occur before forming $CaB_{12}H_{12}$ in the decomposition sequence. And, we also note that even using our lowest-energy CaB_2H_2 structure, the reaction (4) involving this intermediate is ~50 kJ/mol above the decomposition convex hull (Fig. 4). Based on the convex hull definition, this indicates that CaB_2H_2 is not a stable decomposition product but rather is unstable with respect to phase separation into the neighboring phases on the convex hull: $CaB_{12}H_{12}$ and CaB_6. So, the reaction pathway involving the CaB_2H_2 phase is thermodynamically unstable.

Next, we focus on the reactions found to lie on the convex hull involving CaB_2H_6—[reaction (6)], $CaB_{12}H_{12}$—[reaction (3)], and CaB_6—[reaction (2)]. We further investigate the thermodynamic stability of these reactions [(2), (3), and (6) in Table III] by including the vibrational entropy and free-energy (including zero-point energy, ZPE) contributions for all phases in these reactions. Including these vibrational contributions, the difference of reaction enthalpies between $CaB_{12}H_{12}$—[reaction (3)] and CaB_2H_6—[reaction (6)] is ~1 kJ/(mol H_2) for either $T=0$ K or 300 K (Table III). This small energy difference is already beyond the accuracy of our DFT calculations. Thus, the two reaction pathways are essentially degenerate within ~1 kJ/(mol H_2).

In principle, using enthalpies alone to determine the reaction sequence (Fig. 4) is an approximation, because in the Gibbs free energy, the entropies (Table III) of the various reactions may be slightly different from one another, shifting the points in Fig. 4 by various amounts $T\Delta S$. In many cases, the total reaction entropies are roughly equal for all competing reactions, e.g., ~100 J/(K mol H_2) in Table III. This constant entropy would only cause a linear shift of all points in Fig. 4, which would not affect the convex hull, and hence, would not qualitatively affect the stable reaction sequence. However, in this work, we see from Table III that the competing reactions are all extremely close in enthalpy, so even

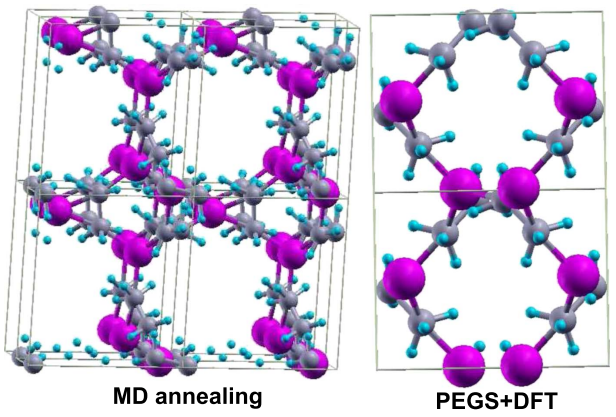

FIG. 5. (Color online) Schematic view of MgB_2H_6 structures from MD annealing simulations of Ref. 15 (the left panel) and from our PEGS+DFT (the right panel). The big red spheres represent Mg atoms. We find our PEGS+DFT structure is ~13 kJ/(mol f.u.) lower in energy than the structure proposed in Ref. 15 but neither forms a stable intermediate in the decomposition of $Mg(BH_4)_2$.

small entropic differences between the various reactions can change the relative order of stability. We see in Table III that the enthalpies of the decomposition reactions to CaB_2H_6 and $CaB_{12}H_{12}$ are degenerate to within ~1 kJ/(mol H_2), but taking into account the entropy, the reaction involving $CaB_{12}H_{12}$—[reaction (3)] is predicted to occur at a slightly lower temperature than the reaction involving CaB_2H_6—[reaction (6)]. These differences are still small and so within the errors associated with the DFT calculations, we can still only assert that our calculations predict that the two competing reactions are essentially degenerate.

VI. MgB_2H_6 DECOMPOSITION PATHWAYS

Having discussed the decomposition of $Ca(BH_4)_2$, we next turn to the isoelectronic compound, $Mg(BH_4)_2$. For Mg-borohydride, the $MgB_{12}H_{12}$ intermediate phase has been observed experimentally and also confirmed theoretically.[13,17] To our knowledge, no other intermediates have been experimentally observed in this system. However, a recent DFT molecular-dynamics (MD) study by van Setten *et al.*[15] has predicted the existence of a metastable intermediate product (MgB_2H_6). In Ref. 15, one H atom is removed from each $[BH_4]^-$ unit in the $Mg(BH_4)_2$ crystal structure and after MD annealing simulations, two $[BH_3]^-$ units bind with each other to form a $[B_2H_6]^{2-}$ unit. We note that this is the same stoichiometry as we obtained in our Ca-borohydride study, however the crystal structure[38] (the left panel in Fig. 5) in Ref. 15 is different than our proposed CaB_2H_6 structure. The method of Ref. 15 relies on an MD annealing study to find candidate structures. However, due to the very short-time scales accessible to MD simulations, this type of approach cannot explore a large number of possible structures in the configurational space of all atomic positions. Hence, it is quite likely that such an MD-based approach would only approach a local minima nearby to the initial configuration.

TABLE IV. PEGS+DFT predicted crystal structures of *Cc* MgB_2H_6 (space group 9, the right panel in Fig. 5). Its lattice parameters are: a=7.25 Å, b=8.52 Å, c=7.86 Å, β=63.79°.

Atom	Wyckoff position	x	y	z
			Cc MgB_2H_6	
Mg	4*a*	0.9890	0.6246	0.9905
B	4*a*	0.0533	0.5626	0.6758
B	4*a*	0.2374	0.3045	0.1812
H	4*a*	0.8780	0.5559	0.8104
H	4*a*	0.0198	0.6030	0.5412
H	4*a*	0.1213	0.4266	0.6586
H	4*a*	0.9054	0.1516	0.5570
H	4*a*	0.2694	0.7065	0.8239
H	4*a*	0.6921	0.3310	0.6544

To try and more effectively search for low-energy structures at this composition, we used the PEGS+DFT method to explore low-energy structures of MgB_2H_6 with the same setup as in the CaB_2H_6 simulations. The PEGS+DFT output MgB_2H_6 structure (the right panel in Fig. 5, Table IV) is 13 kJ/(mol f.u.) lower in energy than the structure found in Ref. 15. In this structure, the bond lengths of B-H are ~1.23 Å and B-B is 1.76 Å, which are similar to those in CaB_2H_6 as well as the MgB_2H_6 structure found from MD by van Setten *et al.* Unlike the MD-structure,[38] the Mg-B bond lengths in the PEGS+DFT structure are nearly constant, ~2.35 Å. They are shorter than the Ca-B in CaB_2H_6 due to the smaller cation radius of Mg ($R_{Mg}<R_{Ca}$).

We next investigate the thermodynamics of three possible decomposition reactions for $Mg(BH_4)_2$. These three reactions [(7)–(9) in Table III] involve decomposition of the borohydride into MgB_2, $MgB_{12}H_{12}$, and MgB_2H_6, respectively. For each case, we calculate the reaction enthalpies with and without vibrational contributions as we did in the case of $Ca(BH_4)_2$ decomposition. From the $Mg(BH_4)_2$ thermodynamic decomposition plot (the lower panel in Fig. 4), we see that both $MgB_{12}H_{12}$—[reaction (8)] and MgB_2—[reaction (7)] lie on the stable decomposition convex hull. However, the hypothetical decomposition involving MgB_2H_6—[reaction (9)] is above the hull in all cases, which indicates that MgB_2H_6 is thermodynamically unstable with respect to decomposition into $Mg(BH_4)_2$ and $MgB_{12}H_{12}$, in the convex hull (the lower panel in Fig. 4). Clearly, MgB_2H_6 is not a stable intermediate in the decomposition of $Mg(BH_4)_2$. Our results confirm the stability of the $MgB_{12}H_{12}$ intermediate, suggested previously.[13,17]

VII. SUMMARY

We have used a combination of DFT calculations and the MC-based PEGS method to study the decomposition pathways and products of both Ca- and Mg-borohydride. The experimentally proposed CaB_2H_2 geometry structure is extremely high in energy and is hence highly unstable. After systematically searching for low-energy structures of

CaB_2H_n ($n=2,4,6$) stoichiometries by PEGS+DFT simulations, we find CaB_2H_2 and CaB_2H_4 crystal structures that do not lie on the lowest energy decomposition path and hence are unstable with respect to $CaB_{12}H_{12}$ phase. However, for $n=6$, we predict a CaB_2H_6 compound which forms a low-energy intermediate in the borohydride decomposition pathway. This new reaction pathway is practically degenerate with decomposition into a previously proposed $CaB_{12}H_{12}$ phase. Similar calculations for the Mg system show that the MgB_2H_6 predicted structures do not form a stable intermediate in the decomposition of $Mg(BH_4)_2$.

ACKNOWLEDGMENTS

Y.Z., C.W., and V.O. gratefully acknowledge financial support from the U.S. Department of Energy under Grant No. DE-FC36-08GO18136 and funding from Ford Motor Co. under the University Research Program. E.H.M. acknowledges financial support from the Department of Energy, office of Energy Efficiency and Renewable Energy under Contract No. DE-AC04-94AL85000. V.O. acknowledges resources of the National Energy Research Scientific Computing Center (NERSC).

[1] Y. Nakamori, K. Miwa, A. Ninomiya, H. Li, N. Ohba, S. I. Towata, A. Züttel, and S. I. Orimo, Phys. Rev. B **74**, 045126 (2006).
[2] J. Yang, A. Sudik, C. Wolverton, and D. J. Siegel, Chem. Soc. Rev. **39**, 656 (2010).
[3] N. Ohba, K. Miwa, M. Aoki, T. Noritake, S. I. Towata, Y. Nakamori, S. I. Orimo, and A. Züttel, Phys. Rev. B **74**, 075110 (2006).
[4] Y. Filinchuk, D. Chernyshov, and R. Cerny, J. Phys. Chem. C **112**, 10579 (2008).
[5] N. A. Zarkevich and D. D. Johnson, Phys. Rev. Lett. **100**, 040602 (2008).
[6] K. Miwa, N. Ohba, S. I. Towata, Y. Nakamori, and S. I. Orimo, Phys. Rev. B **69**, 245120 (2004).
[7] V. Ozolins, E. H. Majzoub, and C. Wolverton, Phys. Rev. Lett. **100**, 135501 (2008).
[8] X.-F. Zhou, Q.-R. Qian, J. Zhou, B. Xu, Y. Tian, and H.-T. Wang, Phys. Rev. B **79**, 212102 (2009).
[9] K. Miwa, M. Aoki, T. Noritake, N. Ohba, Y. Nakamori, S. I. Towata, A. Züttel, and S. I. Orimo, Phys. Rev. B **74**, 155122 (2006).
[10] T. Noritake, M. Aoki, M. Matsumoto, K. Miwa, S. Towata, H.-W. Li, and S. Orimo, J. Alloys Compd. **491**, 57 (2010).
[11] Y.-S. Lee, Y. Kim, Y. W. Cho, D. Shapiro, C. Wolverton, and V. Ozoliņš, Phys. Rev. B **79**, 104107 (2009); E. H. Majzoub and E. J. Ronnebro, J. Phys. Chem. C **113**, 3352 (2009).
[12] L. Schlapbach and A. Züttel, Nature (London) **414**, 353 (2001).
[13] V. Ozoliņš, E. H. Majzoub, and C. Wolverton, J. Am. Chem. Soc. **131**, 230 (2009).
[14] M. D. Riktor, M. H. Sørby, K. Chłopek, M. Fichtner, and B. C. Hauback, J. Mater. Chem. **19**, 2754 (2009).
[15] M. J. van Setten, W. Lohstroh, and M. Fichtner, J. Mater. Chem. **19**, 7081 (2009).
[16] Y. Kim, D. Reed, Y. Lee, J. Y. Lee, J. Shim, D. Book, and Y. W. Cho, J. Phys. Chem. C **113**, 5865 (2009).
[17] S. Hwang, R. C. Bowman, J. J. W. Reiter, J. Rijssenbeek, G. L. Soloveichik, J. Zhao, H. Kabbour, and C. C. Ahn, J. Phys. Chem. C **112**, 3164 (2008).
[18] R. B. King, J. Organomet. Chem. **635**, 75 (2001).
[19] T. P. Fehlner, J. Organomet. Chem. **694**, 1671 (2009).
[20] K. Wade, *Electron Deficient Compounds* (Nelson, New York, 1971).
[21] J. Her, W. Zhou, V. Stavila, C. M. Brown, and T. J. Udovic, J. Phys. Chem. C **113**, 11187 (2009).
[22] J. Y. Lee, D. Ravnsbæk, Y. Lee, Y. Kim, Y. Cerenius, J. Shim, T. R. Jensen, N. H. Hur, and Y. W. Cho, J. Phys. Chem. C **113**, 15080 (2009).
[23] E. H. Majzoub and V. Ozoliņš, Phys. Rev. B **77**, 104115 (2008).
[24] G. Kresse and D. Joubert, Phys. Rev. B **59**, 1758 (1999).
[25] J. P. Perdew, K. Burke, and M. Ernzerhof, Phys. Rev. Lett. **77**, 3865 (1996).
[26] H. J. Monkhorst and J. D. Pack, Phys. Rev. B **13**, 5188 (1976).
[27] C. Wolverton, V. Ozoliņš, and M. Asta, Phys. Rev. B **69**, 144109 (2004).
[28] C. Wolverton and V. Ozoliņš, Phys. Rev. B **75**, 064101 (2007).
[29] C. Kittel, *Introduction to Solid State Physics*, 8th ed. (Wiley, New York, 2005).
[30] M. W. Schmidt, K. K. Baldridge, J. A. Boatz, S. T. Elbert, M. S. Gordon, J. Jensen, S. Koseki, N. Matsunaga, K. A. Nguyen, S. Su, T. L. Windus, M. Dupuis, and J. A. Montgomery, J. Comput. Chem. **14**, 1347 (1993).
[31] L. Wang, D. D. Graham, I. M. Robertson, and D. D. Johnson, J. Phys. Chem. C **113**, 20088 (2009).
[32] H. C. Longuet-Higgins and R. P. Bell, J. Chem. Soc. **1943**, 250.
[33] K. Hedberg and V. Schomaker, J. Am. Chem. Soc. **73**, 1482 (1951).
[34] E. H. Majzoub, K. F. McCarty, and V. Ozoliņš, Phys. Rev. B **71**, 024118 (2005).
[35] R. A. Godfroid, T. G. Hill, T. P. Onak, and S. G. Shore, J. Am. Chem. Soc. **116**, 12107 (1994).
[36] S. Cui, W. Feng, H. Hu, Z. Feng, and Y. Wang, Solid State Commun. **148**, 403 (2008).
[37] J. Bergsma and B. O. Loopstra, Acta Crystallogr. **15**, 92 (1962).
[38] The MgB_2H_6 crystal structure proposed in Ref. 15 (the left panel in Fig. 5) has the following bond lengths: 2.30/2.36/2.41 Å Mg-B, ~1.24 Å B-H, and 1.77 Å B-B.